Convergence and Technologies

Cancer Research

Determination of Tumor Margins with Surgical Specimen Mapping Using Near-Infrared Fluorescence

Rebecca W. Gao[1], Nutte T. Teraphongphom[2], Nynke S. van den Berg[2], Brock A. Martin[3], Nicholas J. Oberhelman[2], Vasu Divi[2], Michael J. Kaplan[2], Steven S. Hong[2], Guolan Lu[2], Robert Ertsey[2], Willemieke S.F.J. Tummers[4], Adam J. Gomez[3], F. Christopher Holsinger[2], Christina S. Kong[3], Alexander D. Colevas[5], Jason M. Warram[6], and Eben L. Rosenthal[2]

Abstract

For many solid tumors, surgical resection remains the gold standard and tumor-involved margins are associated with poor clinical outcomes. Near-infrared (NIR) fluorescence imaging using molecular agents has shown promise for *in situ* imaging during resection. However, for cancers with difficult imaging conditions, surgical value may lie in tumor mapping of surgical specimens. We thus evaluated a novel approach for real-time, intraoperative tumor margin assessment. Twenty-one adult patients with biopsy-confirmed squamous cell carcinoma arising from the head and neck (HNSCC) scheduled for standard-of-care surgery were enrolled. Cohort 1 ($n = 3$) received panitumumab-IRDye800CW at an intravenous microdose of 0.06 mg/kg, cohort 2A ($n = 5$) received 0.5 mg/kg, cohort 2B ($n = 7$) received 1 mg/kg, and cohort 3 ($n = 6$) received 50 mg. Patients were followed 30 days postinfusion and adverse events were recorded. Imaging was performed using several closed- and wide-field devices. Fluorescence was histologically correlated to determine sensitivity and specificity. *In situ* imaging demonstrated tumor-to-background ratio (TBR) of 2 to 3, compared with *ex vivo* specimen imaging TBR of 5 to 6. We obtained clear differentiation between tumor and normal tissue, with a 3-fold signal difference between positive and negative specimens ($P < 0.05$). We achieved high correlation of fluorescence intensity with tumor location with sensitivities and specificities >89%; fluorescence predicted distance of tumor tissue to the cut surface of the specimen. This novel method of detecting tumor-involved margins in surgical specimens using a cancer-specific agent provides highly sensitive and specific, real-time, intraoperative surgical navigation in resections with complex anatomy, which are otherwise less amenable to image guidance.

Significance: This study demonstrates that fluorescence can be used as a sensitive and specific method of guiding surgeries for head and neck cancers and potentially other cancers with challenging imaging conditions, increasing the probability of complete resections and improving oncologic outcomes. *Cancer Res; 78(17); 5144–54. ©2018 AACR.*

Introduction

Surgical resection remains the primary treatment for many solid tumors, and failure to pinpoint residual neoplastic tissue results in positive surgical margins, which are correlated with locoregional recurrence and poor patient outcomes, emphasizing the need for improved intraoperative identification of tumor-involved margins (1–3).

Surgeries for squamous cell carcinomas of the head and neck (HNSCC) may especially benefit from real-time tumor discrimination due to the unforgiving nature of tumor margins in complex head and neck anatomy. If the resection is too conservative, the patient may suffer local recurrence from residual tumor, too aggressive, and critical functional and aesthetic features of the face may be compromised. Currently, intraoperative margin assessment relies on frozen analysis of select tissue specimens, a time-intensive method that can only sample a small portion of the wound bed or the primary specimen and is limited to certain tissue types.

There have been several attempts in different cancer types at developing suitable techniques for the real-time assessment of tumor margins, including radiofrequency spectroscopy, Raman spectroscopy, photoacoustics, optical coherence tomography, Cerenkov luminescence using fluorodeoxyglucose (FDG) tracers, and sheet light microscopy, among others (4–6). These methods all have their own challenges and limitations. Notably, these methods have largely focused on *in situ* imaging of tumor tissue during resection.

[1]Stanford University School of Medicine, Stanford, California. [2]Department of Otolaryngology – Head and Neck Surgery, Stanford University, Stanford, California. [3]Department of Pathology, Stanford University, Stanford, California. [4]Department of Surgery, Leiden University Medical Center, Leiden, the Netherlands. [5]Department of Medicine, Division of Oncology, Stanford University, Stanford, California. [6]Department of Otolaryngology, University of Alabama at Birmingham, Birmingham, Alabama.

Note: Supplementary data for this article are available at Cancer Research Online (http://cancerres.aacrjournals.org/).

Corresponding Author: Eben L. Rosenthal, Stanford University, CC-2213, 1720 2nd Ave S, Stanford, CA 94305. Phone: 205-996-5009; Fax: 205-934-3993; E-mail: elr@stanford.edu

doi: 10.1158/0008-5472.CAN-18-0878

Although HNSCC resections may especially benefit from fluorescence guidance, they are also uniquely challenging for optical imaging due to the orientation difficulties created by complex and heterogeneous topography and interference from shadowing, especially within the oral cavity (7). As such, in the case of head and neck cancers and other cancers with difficult *in situ* imaging conditions, surgical value may primarily lie in the fluorescence evaluation of surgical specimens.

Conveniently, over 90% of HNSCCs overexpress the EGFR, presenting an attractive, cancer-specific target for contrast agents (8). EGFR is a transmembrane cell surface glycoprotein frequently overexpressed in many other types of solid tumors as well, broadening its oncologic applicability (9). We conjugated the therapeutic anti-EGFR antibody panitumumab to a near-infrared (NIR) fluorescent dye and evaluated panitumumab-IRDye800CW in a dose escalation clinical trial. We chose to repurpose an FDA-approved therapeutic agent for imaging given the already-demonstrated safety, regulatory efficiency, cost savings, and promising in-human results (10–14).

Panitumumab is a fully humanized monoclonal IgG2 antibody that binds to the extracellular domain of EGFR with high affinity, and it was first FDA approved in 2006 for metastatic colorectal cancer (15, 16). Preclinical research with panitumumab-IRDye800CW showed high tumor-to-background ratios (TBR) and the ability to detect microscopic areas of disease invisible to the naked eye (16, 17). Previous research on another anti-EGFR antibody, cetuximab-IRDye800CW, demonstrated promising results, and, due to the higher binding affinity and improved safety profile of panitumumab, we chose panitumumab-IRDye800CW to evaluate a new, innovative method of utilizing fluorescence for tumor discrimination and tumor mapping of surgical specimens (18).

The primary aims of our study were to provide evidence of safety, tumor-specific uptake, and assessment of tumor-involved margins in surgical specimens versus *in situ* imaging using an intravenously administered panitumumab-IRDye800CW in patients with HNSCC.

Patients and Methods

Study design

We performed a single-center, nonrandomized, prospective phase I study. The study protocol was approved by the Stanford University Institutional Review Board (IRB 35064) and the FDA (NCT 02415881), and written informed consent was obtained from all patients. The study was performed in accordance with the Declaration of Helsinki, FDA's ICH-GCP guidelines, and United States Common Rule.

All adult patients with biopsy-proven, primary or recurrent HNSCC scheduled to undergo standard-of-care surgery with curative intent were eligible. Exclusion criteria included a life expectancy of less than 12 weeks, a Karnofsky performance status <70%, prior infusion reactions to mAbs, QT prolongation on screening electrocardiogram (ECG; >440 ms in males, and >450 ms in females), significant cardiopulmonary or liver disease, abnormal electrolyte values, and/or utilization of class IA or class III antiarrhythmic agents.

Four cohorts of patients were enrolled in this dose escalation study. Cohort 1 ($n = 3$) received a microdose of 0.06 mg/kg (1/100 of one therapeutic panitumumab dose) and was primarily assessed for safety. Cohort 1 was not included in the statistical analysis and served only as a negative reference point, as the devices were insufficiently sensitive to detect this concentration level of dye. Cohort 2 was used to assess for ranging dose. Cohort 2A ($n = 5$) received a loading dose of 100 mg of unlabeled panitumumab, followed by a 0.5 mg/kg (1/12 of therapeutic) infusion of the study drug, conjugated panitumumab-IRDye800CW. Cohort 2B ($n = 7$) received the same loading dose as cohort 2A and an infusion of 1 mg/kg (1/6 or therapeutic) of panitumumab-IRDye800CW. Cohort 3 ($n = 6$) received a fixed dose of 50 mg of panitumumab-IRDye800CW. Preclinical research suggested the utility of a loading dose for improved tissue contrast, and we thus examined dosages both with and without a loading dose, as flat dosing may simplify dosing and minimize costs (19).

Briefly, patients were infused with the study drug 1 to 5 days prior to surgery, fluorescence imaging was obtained both of the surgery and of the surgical specimens intraoperatively, and final pathology correlation was obtained (Fig. 1A–D).

Panitumumab-IRDye800CW conjugation

Panitumumab-IRDye800 was produced under GMP at the Leidos Biomedical Research Center (Frederick, MD). IRDye800CW-NHS (IRDye800CW-*N*-hydroxysuccinimide ester; LI-COR Biosciences) was used as a fluorescent probe with a NIR absorption and emission peak of 778 nm/794 nm as discussed previously (17, 20, 21). Briefly, panitumumab (Vectibix; Amgen; 147 kDa) was conjugated to IRDye800CW-NHS by a 2-hour incubation at 20°C in the dark with a dye-to-protein ratio of 2.3:1. Quality control of the conjugate included analysis of drug product in a sterile vial for particulates and integrity of the sterilizing filter. Upon production and vialing, vials were transported to Stanford University (Stanford, CA) where they were stored at the Stanford Health Care Investigational Pharmacy.

Safety assessment

Adverse events were categorized according to the NCI Common Terminology Criteria (version 4.0). Safety data and adverse events were collected at 15 days, and patients were followed for 30 days postinfusion. General physical exam and Karnofsky performance status were assessed prior to enrollment and on the day of surgery, day 15, and day 30. Serum chemistry, metabolic panels, complete blood count, prothrombin/partial thromboplastin times, and thyroid-stimulating hormone levels were obtained on day 0, day of surgery, and as needed for up to 30 days after drug infusion. ECGs were performed at screening, 30 minutes postinfusion of the unlabeled antibody loading dose, 2 hours postinfusion of the antibody–dye complex, and day 30.

Intraoperative NIR imaging

Intraoperative imaging was performed using two wide-field optical imaging systems modified for IRDye800 fluorescence imaging: PINPOINT (Novadaq), and SurgVision Explorer Air (SurgVision BV). During surgery, NIR imaging of the primary tumor was performed prior to and during tumor resection. After tumor removal, the wound bed was imaged. The surgeon then obtained tissue specimens from the wound bed at select margin areas most suspicious for residual tumor involvement according to clinical judgment. In patients undergoing neck dissections, we imaged the lymph nodes and postdissection wound bed. Our protocol stipulated that imaging data would not guide the surgical procedure, and all resections were performed per standard of care.

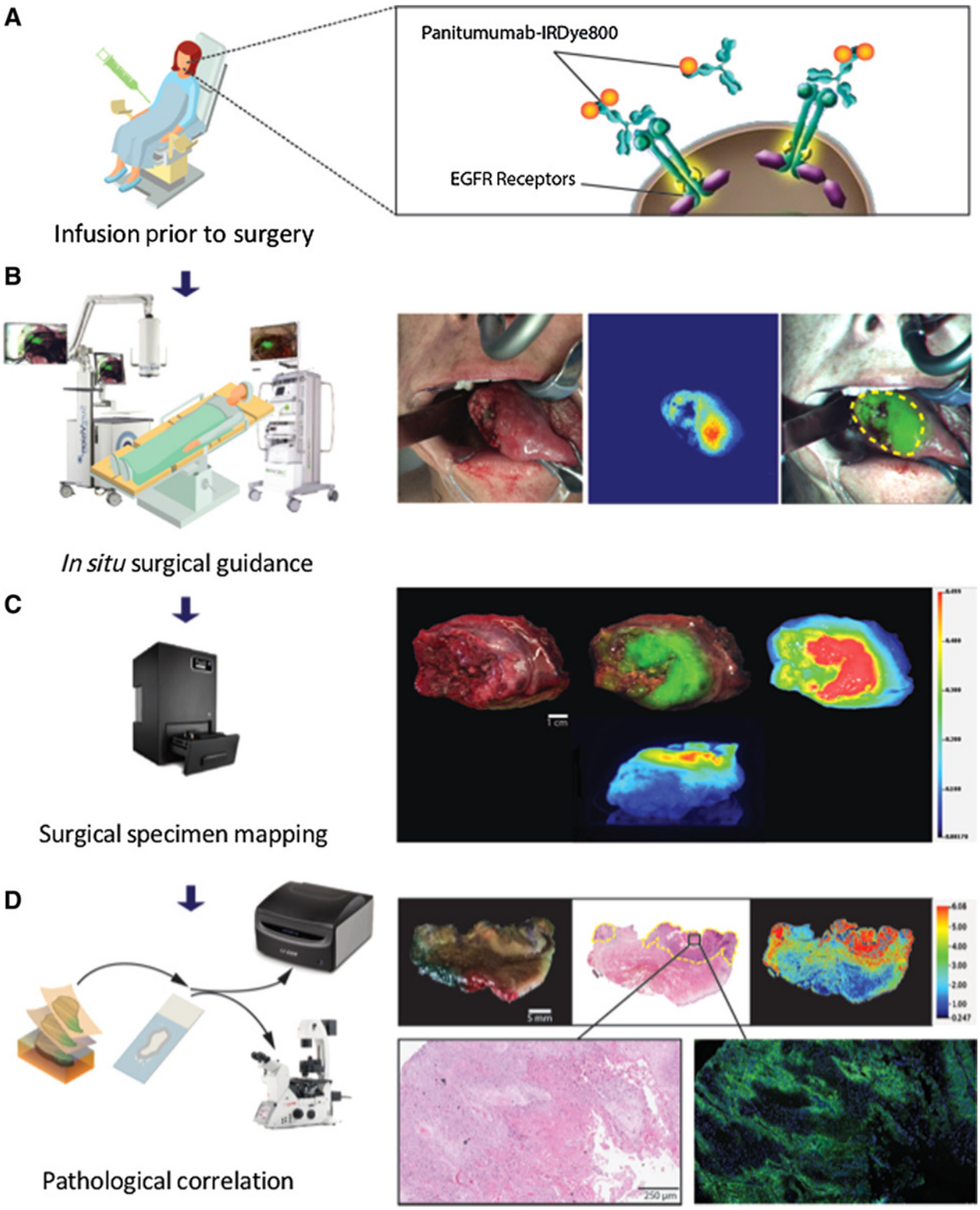

Figure 1.
Clinical workflow. The patient is intravenously infused with the panitumumab-IRDye800CW 1 to 5 days prior to surgery (**A**). During surgery, *in situ* fluorescence imaging is obtained intraoperatively with open-field imaging devices (**B**). Closed-field fluorescence imaging of the surgical specimens is also performed (**C**). After surgery, all surgical specimens undergo standard histopathologic analysis, and fluorescence intensity is compared with EGFR expression and tumor location (**D**).

To minimize ambient lighting, overhead, head-lamp, and room lights were turned off for imaging.

All patient specimens (including the primary tumor specimen, wound bed margins, and lymph nodes) were imaged on the OR back table immediately after resection. Imaging was performed using a closed-field NIR optical imaging system (Pearl Triology imaging platform; LI-COR Biosciences; 800 nm channel) and the two wide-field imaging devices previously described. Images from the open-field devices were immediately available on the screen in real time as a continuous video. The images for the closed-field device (i.e., PEARL) took approximately 15 seconds to capture.

Histopathology processing

The surgical specimens were processed for frozen section or formalin fixation by the pathologist. Select wound bed margins underwent frozen section analysis and the specimens were exhausted. All other specimens were fixed in formalin. After formalin fixation, the primary tumor was sliced at 5-mm intervals and sectioned to fit in cassettes. The cassettes were imaged with a closed-field NIR optical imaging system (Pearl Triology imaging platform; LI-COR Biosciences; 800 nm channel) for measuring fluorescence signal. The specimens in the cassettes were embedded in paraffin for standard histologic processing.

Formalin-fixed paraffin-embedded (FFPE) specimen blocks were serially sectioned at 5-μm thickness. The slides were dried overnight at 37°C and baked for 2 hours at 65°C. Both FFPE blocks and slides were scanned for NIR fluorescence using the Odyssey CLx scanning system (LI-COR Biosciences), using the 800-nm channel, at 21-μm lateral spatial resolution and the highest quality setting.

IHC

FFPE tissue slides were deparaffinized with xylene and rehydrated in 100%/70%/50% concentration ethanol. One slide from each FFPE block was stained with hematoxylin and eosin (H&E) according to standard procedure. All slides were examined by a board-certified pathologist to delineate tumor.

In addition, selected blocks were immunohistochemically evaluated for EGFR expression and tumor identification. Briefly, slides were treated with heat-induced antigen retrieval in EDTA-based buffer (pH 9.0) for 15 minutes, followed by endogenous peroxidase blocking for 30 minutes. For EGFR staining, tissue sections were incubated for 2 hours with anti-EGFR primary antibody (clone EP38Y, prediluted; in 0.025 mol/L Tris-HCl, Thermo Fisher Scientific), then followed by a 30-minute incubation with goat anti-rabbit secondary antibody (Vector Laboratories). For cytokeratin (CK) staining, the slides were incubated with the anti-pan cytokeratin mAb AE1/AE3 (ab961, Abcam) and followed by a 30-minute incubation with goat anti-mouse secondary antibody (Vector Laboratories). Both EGFR and CK slides, were treated with streptavidin for 1 hour and ImmPACT DAB Peroxidase (HRP; Vector Laboratories) for 5 minutes. Sections were counterstained with Mayer's hematoxylin, dehydrated in a series of alcohol and xylene, and coverslipped with mounting media. Stained slides were scanned digitally using a whole slide scanner (Hamamatsu NanoZoomer 2.0-RS).

Microscopy fluorescence imaging

For fluorescence microscopy, selected tissue slides were deparaffinized, and the nuclei were counterstained with 4′,6-diamidino-2-phenylindole (DAPI, Prolong Gold, Life Technologies). Stained slides were dried in the dark at 4°C overnight. The slides were imaged using a custom set-up inverted digital fluorescence microscope (DM6B Leica Biosystems) equipped with a highly sensitive Leica DFC9000GTIs camera (4.2M Pixel sCMOS camera), a metal halide LED light source (X-Cite 200DC, Excelitas Technologies) for DAPI imaging, and a xenon arc lamp LB-LS/30 (Sutter Instrument) for NIR imaging of IRDye800. Image acquisition and processing was done through LAS X software (Leica Biosystems). Images were stitched using Adobe Photoshop CS6.0 software.

Data analysis

Image analysis. The images from the wide-field devices were analyzed using ImageJ (version 1.50i, NIH, Bethesda, MD). For imaging data acquired by the SurgVision Explorer device, images were processed into a compatible format using integrated instrument software for the SurgVision (SV_view, SurgVision BV) prior to ImageJ analysis.

For *in situ* imaging of the primary tumor, the TBRs were calculated as fluorescence intensity of the primary tumor divided by the fluorescence intensity of the background (peritumoral area). Peritumoral tissue for *in situ* imaging was standardized and defined as the area immediately adjacent to tumor tissue with the same-sized area as the tumor. The region of interest (ROI) for tumor was determined based on the fluorescence images and confirmed with H&E. Peritumoral tissue was chosen as the background fluorescence to capture a TBR more reflective of realistic views of the tumor during resections.

For the back-table imaging of the lymph nodes and sectioned primary tumor specimens, TBRs were calculated as fluorescence intensity of the entire specimen divided by the fluorescence intensity of a piece of muscle from the patient. Muscle has low EGFR expression and therefore served as a negative control (18). This alternate method was used because tumor versus peritumoral area could not be delineated, because the purpose of pathologic analysis of these specimens is to determine whether or not tumor tissue is involved.

For the back-table imaging of the wound bed margins, TBRs were calculated as fluorescence intensity of the entire specimen divided by average fluorescence intensity of three randomly selected spaces (not including the specimen itself) with the same size as the specimen. This calculation method was used because the wound bed margins are often sent for frozen section pathologic analysis intraoperatively, prior to availability of a muscle specimen for comparison.

Correlation of EGFR expression and fluorescence intensity. To determine the correlation between fluorescence intensity and EGFR expression, three ROIs were randomly drawn based on each IHC-stained EGFR slide. The mean fluorescence intensity (MFI) of the ROIs was measured in a consecutive tissue slide from Odyssey CLX fluorescence scanning system (LI-COR Biosciences) and the system's integrated instrument software (ImageStudio, LI-COR Biosciences). Staining intensities for EGFR in each of the corresponding ROIs were calculated through analysis of whole slide scanned images (Hamamatsu NanoZoomer 2.0-RS). Image analysis was done in ImageJ. Image thresholds and the percentage of EGFR-positive stained area related to the total ROI area were calculated (EGFR-stained area/total ROI area), and a regression line was generated.

Correlation of fluorescence signal with tumor depth. After removal from the patient, the gross primary tumor specimen was imaged by closed-field fluorescence imaging devices of the entire deep margin surface (Supplementary Fig. S2A and S2B). The threshold was calculated using the average of the MFIs of tumor tissue in primary tumor specimens as the standard for tumor tissue fluorescence signal, and we used one half that MFI value as the threshold for fluorescence. All areas on the deep margin surface of the gross specimen exceeding this threshold were considered positive for fluorescence, and all other areas were negative. Pathology slides sectioned from fluorescent areas of the deep margin were considered fluorescence positive.

The distance between the tumor-involved tissue and the deep margin surface of the specimen for each pathology slide was measured using ImageJ for both fluorescence-positive and fluorescence-negative slides. The lateral width of the tumor area was measured and divided into 10 equal intervals (Supplementary Fig. S2C). At the beginning of each interval, the straight-line distance between the tumor-involved area and the deep margin surface was measured for a total of 10 measurements per slide (Supplementary Fig. S2D). The average distances of tumor-involved tissue from the deep margin in fluorescent-positive slides were comparedwith average distances in fluorescence-negative slides using unpaired, two-tailed t tests by patient and by cohort.

Sensitivity and specificity. To determine the sensitivity and specificity of panitumumab-IRDye800CW for surgical specimens, an ROC analysis was performed on data from all tissue specimens submitted for pathologic evaluation. Based on each tissue cassette, we determined the MFI, defined as total counts divided by ROI pixel area. Next, the pathologist, using the corresponding H&E slide as the gold standard, assessed whether or not the tumor was present in the cassette using a binary (yes/no) approach. We calculated the sensitivity and specificity of the fluorescence signal of the formalin-fixed tissues against the H&E result. Gland regions exhibited elevated fluorescence and were excluded.

To determine the sensitivity and specificity for wound bed margin assessment, we used a slightly different approach. Recognizing the importance of sensitivity over specificity (i.e., exclusion of false-negatives), we aimed for maximal sensitivity. The TBRs for each wound bed margin specimen were compared with the pathology diagnosis, and the differences between the TBRs for negative margins and positive margins were analyzed using an unpaired t test (two-tailed). Dysplastic tissue was considered "positive" because it resulted in further surgical resection. Specimens composed completely of bone tissue were excluded due to poor fluorescence penetration. For cohort 3 (50 mg), the primary resecting surgeon was asked to predict whether each margin specimen was involved by malignancy, and the resulting sensitivity and specificity were compared with predictions by the fluorescence imaging.

For the deep margins, the sensitivity and specificity of the fluorescence signal in detecting tumor-involved areas within 1 and 2 mm of the deep margin were calculated in GraphPrism by cohort. One and 2 mm were selected because these are the distances commonly used by pathologists to indicate close and/or negative resection margins for HNSCC.

Statistical analysis

Statistical analysis was performed using a two-way ANOVA for validity of the differences between groups where a single condition changed (version 6.0c, GraphPad Software). Correlations of surgical imaging to quantitative measures of fluorescence in surgical specimens and IHC analyses of specimens were investigated for the purposes of colocalization and correlation (Pearson correlation) and for determination of MFI obtained by fluorescence signal. A P value of 0.05 or less was considered statistically significant.

Results

Safety assessment

From December 2015 to October 2017, 31 patients with biopsy-proven HNSCC were screened for enrollment. Ten patients did not meet eligibility criteria. Patient and tumor characteristics of the remainder 21 patients are summarized in Supplementary Fig. S1. The average age at diagnosis was 62 years old (range, 32–85), and the majority presented with oral cavity SCC (81%). Tumor size (determined by pathology) ranged from 6 to 55 mm (median 32.5 mm) in maximum dimension. Patients in cohort 1 received a microdose (0.06 mg/kg or an average of 4.7 ± 0.7 mg of panitumumab-IRDye800CW), cohort 2A received 0.5 mg/kg (average 39.2 ± 6.9 mg), cohort 2B received 1.0 mg/kg (average 69.1 ± 12.3 mg), and cohort 3 received a fixed 50 mg dose.

No infusion reactions occurred, nor were there any abnormalities in hematology or blood chemistry levels after infusion of panitumumab-IRDye800CW that could be attributed to the study drug. There was a single grade 1–related adverse event in the microdose cohort (0.06 mg/kg); the patient experienced an increase in the QTc interval after infusion of the study drug but returned to baseline at the 30-day follow-up.

Cellular localization of panitumumab-IRDye800CW

In Fig. 2A–F, clear colocalization of fluorescence intensities from fluorescence imaging at 800 nm showed uniform, strong cytoplasmic, and membranous binding of panitumumab-IRDye800CW (green channel) to the tumor cells. This fluorescence was not observed in the normal tissues or the stromal compartment. Regions of high-grade dysplasia showed lower to normal uptake of dye compared with invasive cancer (Fig. 2E and F). DAPI (blue channel) was also used to stain the nuclei of the tissue improve image visualization. To determine the correlation between the fluorescence intensity and tumor location, cytokeratin, and EGFR expression, a board-certified pathologist outlined the areas of tumor (T) and normal tissue (N) on routine H&E slides (Fig. 2G–J). EGFR was highly expressed in tumor tissue and correlated well to high levels of fluorescence; linear regression analysis of percentage of EGFR area and fluorescence revealed a strong correlation ($r^2 = 0.8599$, $P < 0.001$; Fig. 2K).

In situ surgical imaging

Video and still-frame images were obtained during surgery, and, from these images, TBRs were calculated to determine the ability of panitumumab-IRDye800CW to discriminate between normal and tumor tissue (Fig. 3A–D). *In situ* images of the primary tumor were analyzed and plotted by cohort. Average TBR of 2.4 ± 0.4 was found for cohort 2A (0.5 mg/kg), 2.6 ± 0.4 for cohort 2B (1.0 mg/kg), and 2.5 ± 0.4 cohort 3 (50 mg fixed dose). No statistically significant differences were observed between the TBRs of the wide-field devices ($P > 0.05$). In all patients, fluorescence imaging of the surgical specimens confirmed intraoperative

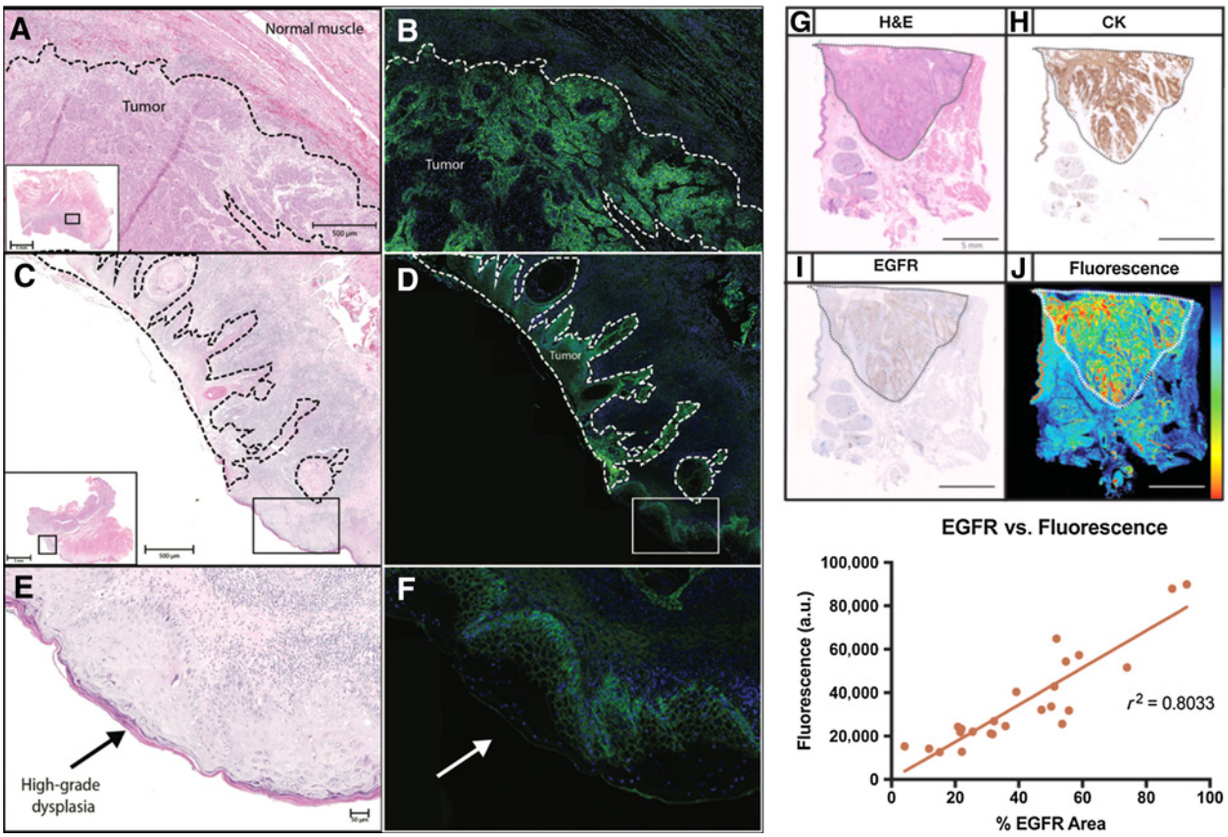

Figure 2.
Target validation. Microscopy images of H&E stains of tumor and normal tissue (**A** and **C**) are compared with images showing EGFR expression (**B** and **D**). Areas of high-grade dysplasia (**E**) show increased EGFR expression (**F**), although less compared with areas of invasive carcinoma. A section of tumor and normal tissue is compared by H&E (**G**), cytokeratin staining (**H**), EGFR expression (**I**), and fluorescence intensity (**J**). EGFR expression shows a strong positive correlation with fluorescence intensity (**K**).

findings. No intraoperative imaging was performed in cohort 1 (0.06 mg/kg panitumumab-IRDye800CW), as the dose was too low for *in situ* imaging, and the primary goal was to determine study drug safety.

Identifying the smallest amount of detectable disease. When evaluating fluorescence intensities of different tissue types in the resected specimens, a strong correlation was found between fluorescence intensities, tissue weight, and tissue type, with r^2 of 0.93, 0.83, and 0.79 for tumor, normal muscle, and normal epithelium, respectively ($P < 0.001$; Fig. 3E and F). Moreover, when looking at the normalized fluorescent signal by weight, a 12-fold increase in fluorescence signal was observed when comparing tumor and normal muscle ($P < 0.0001$). Similarly, a 3-fold fluorescence intensity difference was found between tumor and normal epithelium (which also expresses EGFR; $P = 0.0002$).

Surgical specimen tumor mapping

Tumor detection in the primary tumor specimen. Evaluation of fluorescence intensity immediately after surgical resection and prior to formalin fixation was performed in a closed-field device. A quantitative comparison of MFI of the primary tumor and the enveloping uninvolved tissue (background) and TBRs are shown by cohort (Fig. 3C). There is no statistically significant difference in the background signal from cohorts 2A, 2B, and 3. We achieved average TBRs of 2.67 ± 0.7 for cohort 1 (0.06 mg/kg), 5.40 ± 0.6 for cohort 2A (0.5 mg/kg), 5.44 ± 0.7 for cohort 2B (1.0 mg/kg), and 6.53 ± 1.2 for cohort 3 (50 mg). As expected, in cohort 1 (0.06 mg/kg), minimal fluorescence signal in surgical specimens was detected. The difference in MFIs and TBRs between cohort 1 and the three other cohorts was statistically significant ($P < 0.05$), but there was no difference in TBRs between cohorts 2A, 2B, and 3.

To determine the overall specificity and sensitivity of panitumumab-IRDye800CW for neoplastic tissue, an ROC curve was generated from the MFI data from the specimen cassettes from each patient and plotted as sensitivity versus (1-specificity). Average positive predictive value (PPV), negative predictive value (NPV), and AUC are also displayed (Table 1). All cohorts showed very high sensitivity and NPV (≳90%). Cohorts 2B and 3 both showed higher specificity (91%, 92% vs. 78%) and PPV (86%, 82% vs. 68%) compared with cohort 2A. They also demonstrated higher AUC values (0.95, 0.93 vs. 0.83), although there was no statistical difference between cohorts 2B and 3 compared with cohort 2A ($P = 0.09$, $P = 0.2$).

Tumor detection in margin samples. When strips of tissue were obtained from the wound bed by the surgeon, these samples were imaged prior to frozen sectioning (Fig. 4A). The average TBR of

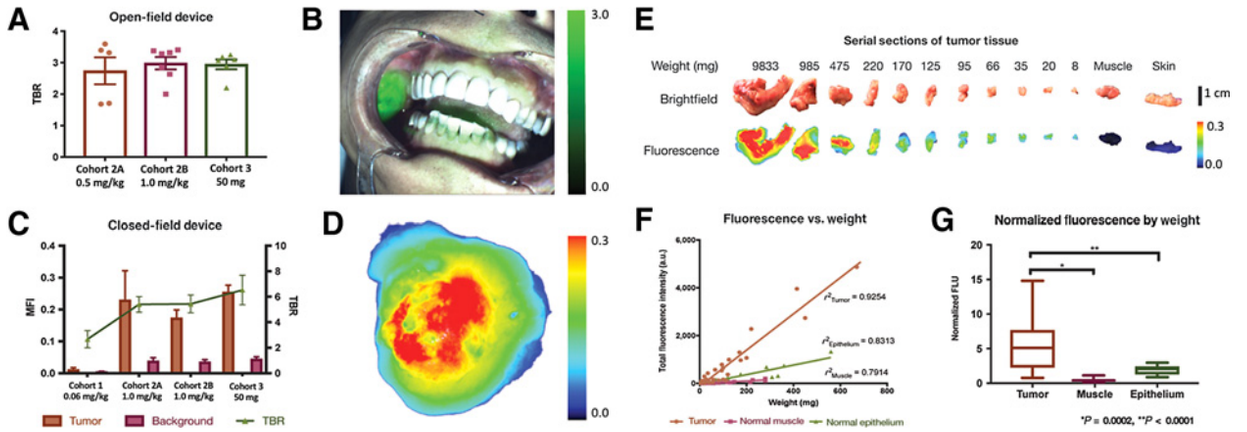

Figure 3.

In situ and surgical specimen mapping. **A,** TBRs by cohort of the *in situ* primary tumor obtained using an open-field device. **B,** An example of an *in situ* image. **C,** MFIs of tumor tissue in the primary tumor surgical specimen and background muscle by cohort obtained using a closed-field imaging device with TBRs. **D,** Sample image of a primary tumor specimen. **E,** Brightfield and fluorescence images of serial sections of tumor tissue, muscle, and skin by weight. **F,** Muscle, normal epithelium, and tumor tissue show positive linear correlation of weight and fluorescence signal. **G,** Normalized fluorescence by weight shows statistically significant difference between fluorescence of tumor compared with muscle and normal epithelial tissue.

positive wound bed samples in cohort 2A was 18.14 and 4.63 for negative margins ($P = 0.0005$; Fig. 4B). The average SBR for positive margins in cohort 3 was 50.27 and 11.12 for negative margins ($P < 0.0001$; Fig. 4C). Only cohorts 2A and 3 had positive wound bed margins for comparison.

In addition, panitumumab-IRDye800CW demonstrated a high sensitivity and specificity for the intraoperative detection of tumor-involved margin samples. In cohort 2A (0.5 mg/kg dose), there was a sensitivity of 100%, a specificity of 90%, an AUC of 0.98 ($P = 0.007$), PPV of 80%, and NPV of 100% (Table 2). For cohort 3 (50 mg dose), there was a sensitivity of 100%, specificity of 74%, AUC of 0.97 ($P = 0.002$), PPV of 52%, and NPV of 100%. Compared with the resecting surgeon, fluorescence signal revealed the presence of disease more consistently: Fluorescence had a much greater sensitivity (100% vs. 36%) and NPV (100% vs. 84%) with less specificity (74% vs. 97%) and PPV (52% vs. 80%).

Mapping tumor depth around the margins of the primary specimen. At the deep surface of the primary tumor specimen, we examined the distance of tumor tissue from the specimen edges using fluorescence. In all three cohorts, fluorescence signal in an area indicated that tumor tissue was significantly closer to the margin edges than in areas without fluorescence ($P < 0.0001$; Fig. 5A–D). There was a significant difference between the tumor distance from the edges of fluorescent areas in cohort 2B compared with 2A and 3 (2A, $P < 0.001$; 3, $P < 0.001$). There was no difference between the tumor distance in fluorescent areas between cohorts 2A and 3 ($P = 1$).

Comparison of tumor tissue depth from the deep margin surface of the primary tumor specimen in fluorescent areas compared with areas without fluorescence was 2.5 ± 2.4 mm versus 7.6 ± 4.9 mm for cohort 2A [$P < 0.0001$, 95% confidence interval (CI), 4.3–5.9], 2.5 ± 1.8 mm versus 6.9 ± 3.5 mm for cohort 2B ($P < 0.0001$; 95% CI, 3.6–5.1), and 3.8 ± 2.5 mm versus 8.6 ± 3.7 mm for cohort 3 ($P < 0.0001$; 95% CI, 5.3–6.2).

Fluorescence had >95% sensitivity and >98% NPV for areas where the tumor tissue was ≤1 mm from the margin edge in all three cohorts 2A, 2B, 3 and 80% to 90% sensitivity and >90% NPV for tumor tissue ≤2 mm (Supplementary Tables S2 and S3). At both the ≤1 mm and ≤2 mm cutoffs, the cohorts showed lower specificity (50%–60%) and PPV (14%–50%). Generally, the ≤2 mm cutoff showed modestly higher specificity and PPV and lower sensitivity and NPV compared with the ≤1 mm cutoff. Cohort 2B demonstrated the lowest specificity and PPV compared with cohort 2A and cohort 3.

Table 1. Sensitivity, specificity, PPV, NPV, and AUC by cohort of the primary specimen shown as average values ± SEM

	Cohort 2A	Cohort 2B	Cohort 3	All cohorts
Dose	0.5 mg/kg	1.0 mg/kg	50 mg	
n	165	550	186	972
Sensitivity (%)	92 ± 3.6	92 ± 2.7	89 ± 5.1	91 ± 2.1
Specificity (%)	78 ± 10.3	91 ± 1.5	92 ± 3.5	88 ± 3.3
PPV	68 ± 11.4	86 ± 8.2	82 ± 9.5	80 ± 4.4
NPV	95 ± 3.5	96 ± 3.1	94 ± 2.8	93 ± 2.0
AUC	0.83 ± 0.07	0.95 ± 0.01	0.93 ± 0.03	0.91 ± 0.02

Discussion

Fluorescently labeled antibodies have been a promising development for achieving tumor-specific, intraoperative guidance for oncologic resections. The focus, however, for optical image-guided surgery has predominantly centered around *in situ* surgical navigation during specimen removal. Experience in recent clinical trials suggests that open-field imaging may have distinct limitations using current hardware, depend on instrument positioning intrusions, and intrude on surgeon workflow (7). HNSCC and other cancers with limited exposure and narrow wound beds that result in difficult imaging conditions may derive more benefit from specimen tumor mapping rather than intermittent *in situ* imaging. To this end, we developed several specimen-mapping strategies to improve real-time information needed by the surgeon that integrates into the workflow of oncologic surgery.

Compared with previous research on other cancer-specific fluorescence tracers, we present two unique methods of utilizing

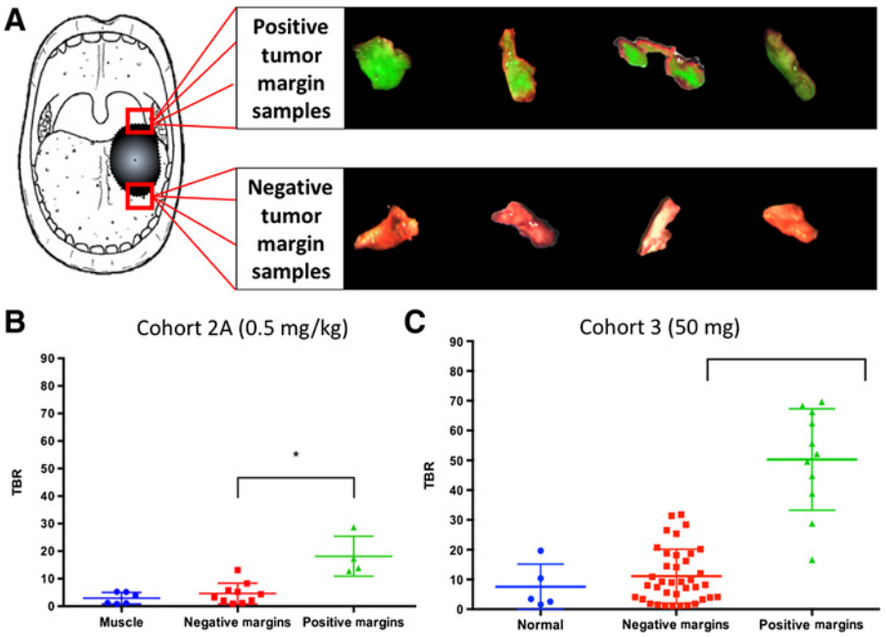

Figure 4.
Margin samples. **A,** Examples of tumor-involved (positive) and normal (negative) margin samples biopsied from the wound bed by the resecting surgeon per clinical judgment. **B** and **C,** TBRs of muscle, negative margin samples, and positive margin samples in cohort 2A (0.5 mg/kg; **B**) and cohort 3 (50 mg; **C**). There is a statistically significant difference between positive and negative margins ($P = 0.0005$; $P < 0.0001$).

fluorescence to detect tumor-involved margins within surgical specimens: screening intraoperative margin samples and identifying close or positive margins on deep margin of the primary tumor specimen (10–14, 18, 22). Margin sampling is an active area of research and controversy, which is a primary driving motivation for our research to improve intraoperative margin analysis through fluorescence imaging. There is significant controversy for which locations in the wound bed and how many locations are necessary to comprehensively determine the presence of residual disease. Surgical margins generally are obtained using two widely accepted methods: The first is the removal of small tissue biopsies from the wound bed by the surgeon. The second is that the entire specimen is examined by the surgeon and/or pathologist after which margins are taken. Thus, margin selection remains a controversial area of surgical oncology, and it is most often that the surgeon chooses the method based on personal preference, clinical circumstance, and institutional bias (23). Sending multiple margin samples is a resource-intensive method that can prolong anesthesia time while waiting for results. Our data show that positive, tumor-involved margin samples are significantly more fluorescent than normal, negative margin samples. Although the specificity is limited (74%–90%), the sensitivity and NPV is exceptionally high (100%, 100%). This enables fluorescence to be an ideal "rule out" test, allowing the clinical team to screen these margin samples and prioritize the fluorescent ones for further examination, leading to savings of time and labor.

Table 2. Sensitivity and specificity of fluorescence for tumor-involved margin samples

	Cohort 2A	Cohort 3	Surgeons
Sensitivity	100%	100%	36%
Specificity	90%	74%	97%
PPV	80%	52%	80%
NPV	100%	100%	84%
AUC	0.98	0.97	N/A

NOTE: Sensitivity, specificity, PPV, NPV, and AUC of fluorescence signal predictions of tumor-involved margin samples in cohort 2A and cohort 3. Fluorescence signal predictions were compared with predictions made by the primary resecting surgeon.

On the other hand, although margin samples are used for the binary evaluation of whether or not tumor tissue is present in the sampled location, the goal for evaluating the primary tumor specimen is altogether different. The presence of tumor in the primary tumor specimen is undisputed, and it is instead necessary to determine resection completeness by examining how closely tumor tissue extends to the specimen edges. The presence of tumor tissue within 1 mm of the specimen surface is generally considered a positive margin, whereas tumor greater than 5 mm away is considered negative. Presence of tumor between 1 and 5 mm from the cut surface is often considered as a close margin. Our data indicate that fluorescence is sensitive for detection of tumor within the 0 to 5 mm range, which has potential future applications in allowing pathologists to prioritize fluorescent areas for further analysis, also leading to savings of time and labor.

Even more specifically, our data suggest that panitumumab-IRDye800CW can distinguish between areas of the primary specimen harboring tumor close to the edges and areas in which tumor is farther away, thus creating a fluorescent "map" predicting tumor depth across the entire surface of the specimen. This mapping capability can also be used to reduce the sampling error inherent to the current standard of sampling areas of the primary tumor specimen or the wound bed to determine the presence of tumor-involved margins. This sampling error may be further worsened by the limited ability of the surgeon to predict (and thus select to sample) areas with tumor-involved margins, as suggested by a 36% surgeon sensitivity for positive margins in our trial. Fluorescence, however, may be able to map out the entire specimen surface (the surgical margin) to identify suspicious areas of residual tumor tissue, as sampling can only inspect a fraction of this space. By using tumor mapping of surgical specimens, fluorescence can potentially assist in achieving complete resections and improved oncologic outcomes.

Our data suggest that, at our current level of technology, closed-field fluorescent tumor mapping of surgical specimens on the OR

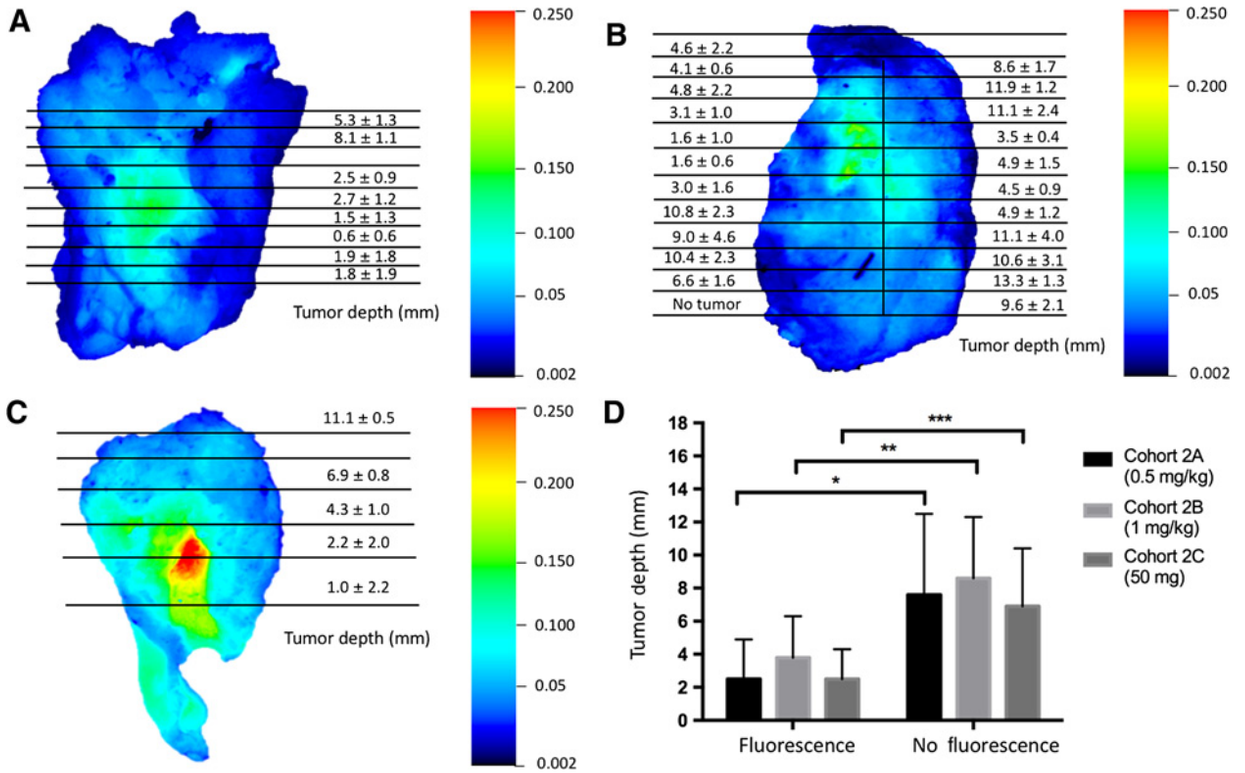

Figure 5.

Tumor mapping of surgical specimens. Distance of tumor tissue to the deep margin surface of the primary tumor specimen given as average tumor depth (mm) ± SD. Views of the entire deep margin surface of representative samples from cohort 2A (**A**), cohort 2B (**B**), and cohort 3 (**C**) are shown here. **D,** Comparison of tumor tissue depth from the deep margin surface of the primary tumor specimen in fluorescent areas versus areas without fluorescence.

back table may provide more consistent data compared with open-field *in situ* imaging. *In situ* surgical imaging requires open-field devices that are subject to interference from ambient light, reflectance, and placement at variable angles to the tumor, whereas back-table imaging of surgical specimens can utilize closed-field devices with a controlled environment. The *in situ* images showed an average TBR of 2.5 compared with 5.8 for the surgical specimen images, in part due to interference from ambient lighting. We attempted to overcome these difficulties by reducing overhead lighting, but this often interrupts surgical workflow, whereas surgical specimen imaging can be performed in parallel on the back table while the surgeons operate, minimizing disruption from maneuvering the imaging devices. These closed-field devices are inexpensive, readily available, and relatively small. Given these advantages, closed-field devices with a controlled, standardized environment and the potential to generate three-dimensional tumor maps of surgical specimens may be an optimal way to leverage current technology.

We validated our results by examining fluorescence signal with tumor and normal tissue by linear weight measurements, and fluorescence intensity also correlated well with EGFR expression and density. Fluorescence signal was shown to be relatively homogeneous across the cytoplasm and cellular membrane of tumor tissue, consistent with the known antibody–receptor complex transition from the cell surface to the cytoplasm (24). Imaging contrast between tumor and normal tissue was consistent with preclinical data (25).

In terms of patient safety, panitumumab-IRDye800CW demonstrated a highly favorable safety profile. There were no infusion reactions, and only one grade 1 adverse event. This shows improved safety over cetuximab-IRDye800CW, a compound we previously used to demonstrate simple, initial feasibility and safety of a fluorescently labeled anti-EGFR antibody (10). When designing this study to evaluate the new methods for surgical specimen mapping we proposed, we chose panitumumab-IRDye800CW instead of cetuximab-IRDye800CW in order to improve patient safety, as panitumumab is a fully humanized mAb, whereas cetuximab is a human–mouse chimera. Accordingly, because we are using much lower doses for imaging compared with the therapeutic dose of panitumumab (which also has a safer profile as a parent compound compared with cetuximab), it is unsurprising to see minimal adverse effects (15, 16).

We also evaluated the optimal dosing necessary to achieve these detection goals. The three cohorts (2A, 2B, 3) did not show significantly different TBRs of the primary tumor specimen. A larger difference between fluorescence of positive and negative wound bed margins in cohort 3 (1 mg/kg) compared with cohort 2A (0.5 mg/kg) suggest that a higher dose may be more effective. However, cohort 2B (1 mg/kg) might have an unnecessarily high dose for mapping tumor depth on the primary specimen. Fluorescence intensity from tumor in cohort 3 (1 mg/kg) was strong enough to be detected at a deeper depth than cohort 3 (0.5 mg/kg) or cohort 3 (50 mg) but had tradeoffs in specificity and PPV. In addition, the loading dose of unlabeled antibody does not appear

to add additional value. As such, cohort 3 (flat dose of 50 mg of panitumumab-IRDy800CW) appears to be the safest and most cost-effective dose.

The primary limitation of our trial is the small cohort sizes that limited the power to distinguish how tumor size and location may affect fluorescence signal. The tumors were not evaluated preoperatively for EGFR status, although we did not see different EGFR expression levels impact TBR on histologic examination. EGFR is also modestly expressed in the basal layer of normal mucosa and skin, which can increase background fluorescence (26). In addition, we did not examine and quantify the histologic characteristics of the resected tumors to assess for aggressive or complex features such as perineural invasion, distant tumor nests, and stromal alterations, which may affect drug uptake. HNSCC also exhibits inter- and intratumor heterogeneity, which we attempted to correct for by using each patient as his/her own control in the analysis.

A physical limitation of the technology is the penetration depth of NIR fluorescence (approximately 5 mm; ref. 27). This depth can identify tumor tissue in small margin samples and at distances relevant for determining resection completeness (0–5 mm) but cannot provide complete internal pictures of large specimens >10 mm in thickness. Compared with other intraoperative imaging methods in development, fluorescence imaging has acceptable penetration depth (compared with 1–2 mm for Cerenkov luminescence with radiotracers), faster imaging speeds (compared with 15–30 minutes for multispectral imaging), lack of ionizing radiation, and high spatial resolution (although less than sheet light microscopy; refs. 4–6, 28). In addition, new combinatory uses of fluorescence in optoacoustics (such as multispectral optoacoustic tomography) have shown potential to incorporate the high image fidelity of optical imaging with the increased penetration depth (3–5 cm) afforded by acoustic technology (28–30).

Overall, our data present a promising new avenue of utilizing fluorescence to identify both the presence of tumor tissue in margin samples as well as to map tumor depth in the primary tumor specimen. Tumor mapping of surgical specimens may be more revealing than *in situ* imaging in cancers with difficult imaging conditions in particular, but margin assessment utilizing the methods presented in this trial may potentially be applicable to all oncologic surgeries. These promising results from conjugating fluorescent dyes to therapeutic mAbs may prove to be a valuable method of combining existing technologies to develop safe, tumor-specific imaging agents to improve intraoperative detection of cancerous tissue to ultimately improve oncologic outcomes.

Conclusions

We present a novel method of detecting tumor-involved margins in surgical specimens using a cancer-specific agent to provide highly sensitive and specific, real-time, intraoperative surgical navigation in resections with complex anatomy otherwise poorly amenable to image guidance.

Disclosure of Potential Conflicts of Interest

F.C. Holsinger is the founder and chief scientific advisor at Surgical Vision Technologies and has ownership interest (including stock, patents, etc.) in Surgical Vision Technologies, Inc. No potential conflicts of interest were disclosed by the other authors.

Authors' Contributions

Conception and design: N.T. Teraphongphom, S.S. Hong, G. Lu, J.M. Warram, E.L. Rosenthal

Development of methodology: R.W. Gao, N.T. Teraphongphom, N.S. van den Berg, N.J. Oberhelman, G. Lu, W.S.F.J. Tummers, A.D. Colevas, J.M. Warram, E.L. Rosenthal

Acquisition of data (provided animals, acquired and managed patients, provided facilities, etc.): R.W. Gao, N.T. Teraphongphom, N.S. van den Berg, B.A. Martin, N.J. Oberhelman, V. Divi, M.J. Kaplan, S.S. Hong, G. Lu, W.S.F.J. Tummers, A.J. Gomez, F.C. Holsinger, C.S. Kong, A.D. Colevas, E.L. Rosenthal

Analysis and interpretation of data (e.g., statistical analysis, biostatistics, computational analysis): R.W. Gao, N.T. Teraphongphom, N.S. van den Berg, S.S. Hong, G. Lu, W.S.F.J. Tummers, A.J. Gomez, A.D. Colevas, J.M. Warram, E.L. Rosenthal

Writing, review, and/or revision of the manuscript: R.W. Gao, N.T. Teraphongphom, N.S. van den Berg, B.A. Martin, N.J. Oberhelman, V. Divi, S.S. Hong, G. Lu, W.S.F.J. Tummers, A.J. Gomez, C.S. Kong, A.D. Colevas, J.M. Warram, E.L. Rosenthal

Administrative, technical, or material support (i.e., reporting or organizing data, constructing databases): R.W. Gao, N.T. Teraphongphom, N.J. Oberhelman, G. Lu, R. Ertsey, E.L. Rosenthal

Study supervision: N.T. Teraphongphom, S.S. Hong, A.D. Colevas, J.M. Warram, E.L. Rosenthal

Acknowledgments

This work was supported by the Stanford Comprehensive Cancer Center, the Stanford University School of Medicine Medical Scholars Program, the Netherlands Organization for Scientific Research (019.171LW.022), and the NIH and the NCI (R01CA190306, R21CA182953, R21CA179171, T32CA091078). Institutional equipment loans were received from Novadaq, SurgVision.

The costs of publication of this article were defrayed in part by the payment of page charges. This article must therefore be hereby marked *advertisement* in accordance with 18 U.S.C. Section 1734 solely to indicate this fact.

Received March 23, 2018; revised May 3, 2018; accepted June 25, 2018; published first July 2, 2018.

References

1. Ganly I, Patel S, Shah J. Early stage squamous cell cancer of the oral tongue – clinicopathologic features affecting outcome. Cancer 2011; 118:101–11.
2. McMahon J, O'Brien CJ, Pathak I, Hamill R, McNeil E, Hammersley N, et al. Influence of condition of surgical margins on local recurrence and disease-specific survival in oral and oropharyngeal cancer. Br J Oral Maxillofac Surg 2003;41:224–31.
3. Ravasz LA, Slootweg PJ, Hordijk GJ, Smit F, van der Tweel I. The status of the resection margin as a prognostic factor in the treatment of head and neck carcinoma. J Craniomaxillofac Surg 1991;19:314–8.
4. St John ER, Al-Khudairi R, Ashrafian H, Athanasiou T, Takats Z, Hadjiminas DJ, et al. Diagnostic accuracy of intraoperative techniques for margin assessment in breast cancer surgery: a meta-analysis. Ann Surg 2017;265: 300–10.
5. Thill M, Röder K, Diedrich K, Dittmer C. Intraoperative assessment of surgical margins during breast conserving surgery of ductal carcinoma *in situ* by use of radiofrequency spectroscopy. Breast 2011;20: 579–80.
6. Grootendorst MR, Cariati M, Pinder SE, Kothari A, Douek M, Kovacs T, et al. Intraoperative assessment of tumor resection margins in breast-conserving surgery using 18F-FDG cerenkov luminescence imaging: a first-in-human feasibility study. J Nucl Med 2017;58:891–8.
7. Moore LS, Rosenthal EL, Chung TK, de Boer E, Patel N, Prince AC, et al. Characterizing the utility and limitations of repurposing an open-field

optical imaging device for fluorescence-guided surgery in head and neck cancer patients. J Nucl Med 2017;58:246–51.
8. Grandis J, Tweardy D. Elevated levels of transforming growth factor α and epidermal growth factor receptor messenger RNA are early markers of carcinogenesis in head and neck cancer. Cancer Res 1993;53:3579–84.
9. Salomon DS, Brandt R, Ciardiello F, Normanno N. Epidermal growth factor-related peptides and their receptors in human malignancies. Crit Rev Oncol Hematol 1995;19:183–232.
10. Rosenthal EL, Warram JM, de Boer E, Chung TK, Korb ML, Brandwein-Gensler M, et al. Safety and tumor specificity of cetuximab-IRDye800CW for surgical navigation in head and neck cancer. Clin Cancer Res 2015; 21:3658–66.
11. Burggraaf J, Kamerling IM, Gordon PB, Schrier L, de Kam ML, Kales AJ, et al. Detection of colorectal polyps in humans using an intravenously administered fluorescent peptide targeted against c-Met. Nat Med 2015;21:955–61.
12. Hoogstins CE, Tummers QR, Gaarenstroom KN, de Kroon CD, Trimbos JB, Bosse T, et al. A novel tumor-specific agent for intraoperative near-infrared fluorescence imaging: a translational study in healthy volunteers and patients with ovarian cancer. Clin Cancer Res 2016;22:2929–38.
13. Lamberts LE, Koch M, de Jong JS, Adams ALL, Glatz J, Kranendonk MEG, et al. Tumor-specific uptake of fluorescent bevacizumab-IRDye800CW microdosing in patients with primary breast cancer: a phase I feasibility study. Clin Cancer Res 2017;23:2730–41.
14. Terwisscha van Scheltinga AG, van Dam GM, Nagengast WB, Ntziachristos V, Hollema H, Herek JL, et al. Intraoperative near-infrared fluorescence tumor imaging with vascular endothelial growth factor and human epidermal growth factor receptor 2 targeting antibodies. J Nucl Med 2011;52:1778–85.
15. Jakobovits A, Amado RG, Yang X, Roskos L, Schwab G. From XenoMouse technology to panitumumab, the first fully human antibody product from transgenic mice. Nat Biotechnol 2007;25:1134.
16. Amado RG, Wolf M, Peeters M, Van Cutsem E, Siena S, Freeman DJ, et al. Wild-Type KRAS is required for panitumumab efficacy in patients with metastatic colorectal cancer. J Clin Oncol 2008;26:1626–34.
17. Heath CH, Deep NL, Sweeny L, Zinn KR, Rosenthal EL. Use of panitumumab-IRDye800 to image microscopic head and neck cancer in an orthotopic surgical model. Ann Surg Oncol 2012;19:3879–87.
18. Yang XD, Jia XC, Corvalan JR, Wang P, Davis CG. Development of ABX-EGF, a fully human antif-EGF receptor monoclonal antibody, for cancer therapy. Crit Rev Oncol Hematol 2001;38:17–23.
19. Moore LS, Rosenthal EL, de Boer E, Prince AC, Patel N, Richman JM, et al. Effects of an unlabeled loading dose on tumor-specific uptake of a fluorescently labeled antibody for optical surgical navigation. Mol Imaging Biol 2017;19:610–6.
20. van Dam GM, Themelis G, Crane LMA, Harlaar NJ, Pleijhuis RG, Kelder W, et al. Intraoperative tumor-specific fluorescence imaging in ovarian cancer by folate receptor-alpha targeting: first in-human results. Nature Med 2011;17:1315–9.
21. Bhattacharyya S, Patel N, Wei L, Riffle LA, Kalen JD, Hill GC, et al. Synthesis and biological evaluation of panitumumab-IRDye800 conjugate as a fluorescence imaging probe for EGFR-expressing cancers. Medchemcomm 2014;5:1337–46.
22. Koch M, de Jong JS, Glatz J, Symvoulidis P, Lamberts LE, Adams AL, et al. Threshold analysis and biodistribution of fluorescently labeled bevacizumab in human breast cancer. Cancer Res 2017;77:623–31.
23. Hinni ML, Ferlito A, Brandwein-Gensler MS, Takes Rp, Silver CE, Westra WH, et al. Surgical margins in head and neck cancer: a contemporary review. Head Neck 2013;35:1362–70.
24. Citri A, Yarden Y. EGF-ERBB signalling: towards the systems level. Nat Rev Mol Cell Biol 2006;7:505–16.
25. Day KE, Sweeny L, Kulbersh B, Zinn KR, Rosenthal EL. Preclinical comparison of Near-Infrared-Labeled cetuximab and panitumumab for optical imaging of head and neck squamous cell carcinoma. Mol Imaging Biol 2013;15:722–9.
26. Uhlen M, Zhang C, Lee S, Sjöstedt E, Fagerberg L, Bidkhori G, et al. A pathology atlas of the human cancer transcriptome. Science 2017;357:pii: eaan2507.
27. Vahrmeijer AL, Frangioni JV. Seeing the invisible during surgery. Br J Surg 2011;98:749–50.
28. McNally LR, Mezera M, Morgan DE, Frederick PJ, Yang ES, Eltoum IE, et al. Current and emerging clinical applications of multispectral optoacoustic tomography (MSOT) in oncology. Clin Cancer Res 2016; 22:3432–9.
29. Langhout GC, Grootendorst DJ, Nieweg OE, Wouters MW, van der Hage JA, Jose J, et al. Detection of melanoma metastases in resected human lymph nodes by noninvasive multispectral photoacoustic imaging. Int J Biomed Imaging 2014;2014:163652.
30. Taruttis A, van Dam GM, Ntziachristos V. Mesoscopic and macroscopic optoacoustic imaging of cancer. Cancer Res 2015;75:1548–59.